

SNAI2-Mediated Repression of *BIM* Protects Rhabdomyosarcoma from Ionizing Radiation

Long Wang¹, Nicole R. Hensch^{1,2}, Kathryn Bondra¹, Prethish Sreenivas^{1,2}, Xiang R. Zhao¹, Jiangfei Chen^{1,3}, Rodrigo Moreno Campos^{1,2}, Kunal Baxi^{1,2}, Angelina V. Vaseva^{1,2}, Benjamin D. Sunkel⁴, Berkley E. Gryder⁵, Silvia Pomella⁶, Benjamin Z. Stanton^{4,7,8}, Siyuan Zheng¹, Eleanor Y. Chen⁹, Rossella Rota⁶, Javed Khan¹⁰, Peter J. Houghton^{1,2}, and Myron S. Ignatius^{1,2}



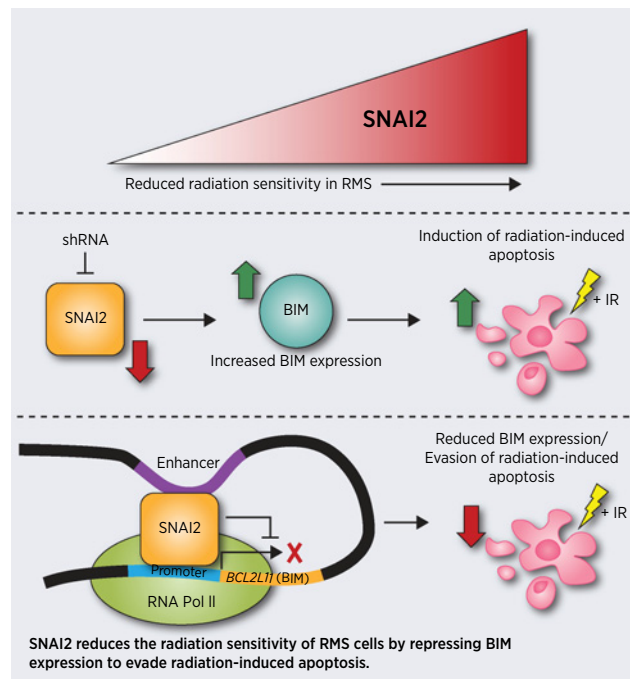
ABSTRACT

Ionizing radiation (IR) and chemotherapy are mainstays of treatment for patients with rhabdomyosarcoma, yet the molecular mechanisms that underlie the success or failure of radiotherapy remain unclear. The transcriptional repressor SNAI2 was previously identified as a key regulator of IR sensitivity in normal and malignant stem cells through its repression of the proapoptotic BH3-only gene *PUMA/BBC3*. Here, we demonstrate a clear correlation between SNAI2 expression levels and radiosensitivity across multiple rhabdomyosarcoma cell lines. Modulating SNAI2 levels in rhabdomyosarcoma cells through its overexpression or knockdown altered radiosensitivity *in vitro* and *in vivo*. SNAI2 expression reliably promoted overall cell growth and inhibited mitochondrial apoptosis following exposure to IR, with either variable or minimal effects on differentiation and senescence, respectively. Importantly, SNAI2 knockdown increased expression of the proapoptotic BH3-only gene *BIM*, and chromatin immunoprecipitation sequencing experiments established that SNAI2 is a direct repressor of *BIM/BCL2L1*. Because the p53 pathway is nonfunctional in the rhabdomyosarcoma cells used in this study, we have identified a new, p53-independent SNAI2/*BIM* signaling axis that could potentially predict clinical responses to IR treatment and be exploited to improve rhabdomyosarcoma therapy.

Significance: SNAI2 is identified as a major regulator of radiation-induced apoptosis in rhabdomyosarcoma through previously unknown mechanisms independent of p53.

Introduction

Ionizing radiation (IR), chemotherapy and surgery comprise the current standard of care for patients with rhabdomyosarcoma, a pediatric malignancy of the muscle, and lead to greater than 70% tumor-free survival in children with this disease (1–3). However,



the survival rate for patients with disease relapse remains dismal at less than 30% (1–4). IR is used to treat both primary tumors and metastatic lesions in patients with relapsed rhabdomyosarcoma (5). Remarkably, these patients often receive a cumulative dose of 36 to 50.4 Gy (5); yet, an understanding of the pathways that regulate the

¹Greehey Children's Cancer Research Institute (GCCRI), UT Health Science Center, San Antonio, Texas. ²Department of Molecular Medicine, University of Texas Health Science Center, San Antonio, Texas. ³School of Environmental Safety and Public Health, Wenzhou Medical University, Wenzhou, Zhejiang, China. ⁴Center for Childhood Cancer and Blood Diseases, Nationwide Children's Hospital, Columbus, Ohio. ⁵Department of Genetics and Genome Sciences, School of Medicine, Case Western Reserve University, Cleveland, Ohio. ⁶Department of Pediatric Hematology and Oncology, Bambino Gesù Children's Hospital, IRCCS, Rome, Italy. ⁷Department of Pediatrics, The Ohio State University College of Medicine, Columbus, Ohio. ⁸Department of Biological Chemistry and Pharmacology, The Ohio State University College of Medicine, Columbus, Ohio. ⁹Department of Laboratory Medicine and Pathology, University of Washington, Seattle, Washington. ¹⁰Genetics Branch, Center for Cancer Research, NCI, NIH, Bethesda, Maryland.

Note: Supplementary data for this article are available at Cancer Research Online (<http://cancerres.aacrjournals.org/>).

L. Wang and N.R. Hensch contributed equally to this article.

Corresponding Author: Myron Ignatius, Greehey Children's Cancer Research Institute, UT Health Science Center, 8403 Floyd Curl, MC 7784, San Antonio, TX 78229. Phone: 210-562-9030; E-mail: ignatius@uthscsa.edu

Cancer Res 2021;81:5451–63

doi: 10.1158/0008-5472.CAN-20-4191

©2021 American Association for Cancer Research

IR-induced DNA damage response (DDR) in rhabdomyosarcoma tumors remains incomplete. In this study, we identify *SNAI2* as a critical radioprotector of rhabdomyosarcoma tumor cells and define the pathways downstream of *SNAI2* signaling that regulate the response to IR in rhabdomyosarcoma.

SNAIL genes comprise a family of transcriptional repressors important for epithelial morphogenesis during development (e.g., the epithelial–mesenchymal transition) and for cell survival (6–8). The role of *SNAI2* in protecting normal hematopoietic stem cells (HSC) from IR-induced apoptosis is well established (9, 10). In radiosensitive cells (e.g., the lymphoid lineage), exposure to IR causes DNA double-strand breaks that trigger the activation of P53. P53-mediated induction of the BH3-only gene *PUMA/BBC3* then leads to mitochondrial apoptosis (11). However, HSCs are uniquely protected from IR-induced apoptosis due to a concomitant P53-mediated induction of *SNAI2* in these cells, which directly represses the expression of *PUMA* (10). Recent studies also implicate *SNAI2* as a regulator of the DDR in normal mammary stem cells (12), and *SNAIL* family members *SNAI1* and *TWIST1* have been shown to regulate the IR-induced DNA damage response in breast cancer cells through regulation of *ZEB1* (13). These studies suggest that the SNAIL family may have widespread importance in regulating the response to IR.

Not surprisingly, adult cancers and relapse disease often present with mutations in or loss of *TP53* (14, 15). In a subset of these tumors that are still radiosensitive, IR has been shown to induce cell death through P53-independent mechanisms involving cell-cycle checkpoint proteins and alternative DDR pathways (reviewed in refs. 16, 17). Interestingly, childhood cancers including rhabdomyosarcoma often retain wild-type (WT) *TP53* (18–21). Mutations in *TP53* account for less than 6% of rhabdomyosarcoma primary tumors, yet they can be acquired during relapse and are associated with a poor outcome (19–21). Because rhabdomyosarcoma tumors harboring either WT or mutant P53 are sensitive to IR (19–21), both P53-dependent and -independent mechanisms of IR-induced cell death appear to be active in this disease. Our analysis show that *SNAI2* protects rhabdomyosarcoma tumors from IR both *in vitro* and *in vivo*. Using rhabdomyosarcoma cell lines that express varying levels of *SNAI2* and a dysfunctional P53 pathway (22, 23), we show that levels of *SNAI2* establish the degree of protection of rhabdomyosarcoma cell lines from IR, regardless of *TP53* mutation status, and that the proapoptotic BH3-only gene *BIM/BCL2L1* is directly repressed by *SNAI2* to confer protection from radiation. Our results suggest that *SNAI2* is a major player in the response to IR in rhabdomyosarcoma and represents a promising target for the radiosensitization of rhabdomyosarcoma tumors during IR therapy.

Materials and Methods

Animals

Animal studies were approved by the University of Texas – Health San Antonio Committee on Research Animal Care under protocol #20150015AR. C.B-Igh-1b/IcrTac-Prkdcscid (SCID) female mice, aged 6 to 8 weeks, were used for *in vivo* xenograft experiments.

Mouse xenograft and *in vivo* IR experiments

Rh30, Rh18, and RD cells with scrambled (shScr), *SNAI2* knockdown (sh*SNAI2*) and RD cells with scrambled (shScr), *SNAI2* knockdown (sh*SNAI2*), *BIM* knockdown (sh*BIM*) and double *BIM/SNAI2* knockdown (sh*BIM/SNAI2*) treatment conditions were collected, counted, and analyzed by flow cytometry to determine viability using

DAPI. Equal numbers of viable cells were then embedded into Matrigel at a final concentration of 1×10^6 (Rh30) or 5×10^6 (Rh18) cells per 100 μ L and injected subcutaneously into anesthetized mice. Tumor growth was monitored and measured weekly using a caliper scale to measure the greatest diameter and length, which were then used to calculate tumor volume. While a subset of tumors was monitored without any treatment, another subset was subjected to low-dose IR therapy for 3 weeks (2 Gy/day; 5 days a week), receiving a total of 30-Gy IR (PXi Precision X-Ray X-RAD 320). Tumor volume was monitored throughout the treatment and during the weeks following treatment. Comparisons between groups were performed using a Student *t* test. Rh18 pBabe and *SNAI2*-Flag xenografts were performed as above, with the treatment arm receiving 2 weeks of IR therapy (2 Gy/day for 5 days/week) for a total of 20 Gy. Relative tumor volume (RTV) was assessed in the RD Scr, *BIM* sh, *BIM/SNAI2* sh1, and *SNAI2* sh1 tumors treated with 30 Gy of radiation and tumor responses were analyzed using the guidelines outlined by Houghton and colleagues (24). Progressive disease (PD): RTV > 0.50 during the study period and RTV > 1.25 at end of study; stable disease (SD): RTV > 0.50 during the study period and RTV \leq 1.25 at end of study; partial response (PR): $0 < \text{RTV} < 0.50$ for at least one time point; complete response (CR): RTV = 0 for at least one time point.

Human rhabdomyosarcoma cell lines

The human rhabdomyosarcoma cell lines RD and SMS-CTR were a gift from Dr. Corinne Linardic, Duke University, Durham, NC. The JR-1 cell line was a gift from Dr. Marielle Yohe, NCI, Frederick, MD. The Rh28, RH30, RH36, Rh41, and Rh18 lines were obtained from P.J. Houghton (GCCRI, San Antonio, TX). All lines except RD and SMS-CTR were maintained in RPMI supplemented with 10% FBS (VWR) at 37°C with 5% CO₂. RD and SMS-CTR cells were maintained in DMEM supplemented with 10% FBS at 37°C with 5% CO₂. Cell lines utilized were between passage 10 and 25. For knockdown assays, cells were not passaged more than 5 passages after stable lines were generated. Cell lines were authenticated by genotyping and short tandem repeat analyses. All rhabdomyosarcoma cell lines were tested and confirmed to be negative for *Mycoplasma*.

Lentiviral/siRNA/retroviral knockdown assays

Scrambled-control and *SNAI2*-specific short hairpin RNA (shRNA) were delivered via the pLKO.1-background vector and packaged using 293T cells. siSlug2 (*SNAI2* sh1) was a gift from Bob Weinberg (Addgene plasmid # 10904; <http://n2t.net/addgene:10904>; RRID:Addgene_10904; ref. 25). siSlug3 (*SNAI2* sh2) was a gift from Bob Weinberg (Addgene plasmid # 10905; <http://n2t.net/addgene:10905>; RRID:Addgene_10905; ref. 25). pMKO shRNA *Bim* was a gift from Joan Brugge (Addgene plasmid # 17235; <http://n2t.net/addgene:17235>; RRID:Addgene_17235; ref. 26). Retroviral particles were made in Plat-A packaging cells using TranstIT-LT1 (Mirus). rhabdomyosarcoma cells were infected with viral particles for 24 hours at 37°C using 8 mg/mL of polybrene (EMD Millipore).

Cell confluence and colony formation assays

Rh18, JR-1, Rh36, RD, SMS-CTR, Rh28, Rh30, and Rh41 parental cells were seeded into 24-well plates at 20% to 50% confluency and stored at 37°C in the Incucyte ZOOM (Essen Bioscience). After 24 hours, cells were subjected to varying degrees of IR (0 Gy–20 Gy) and placed back in the Incucyte. Total confluency over time was monitored every 4 hours over a period of 5 days. Incucyte-confluency assays were performed similarly for scrambled, *SNAI2* shRNA, *TP53* shRNA, *BIM* shRNA, and *SNAI2/BIM* double-knockdown shRNA

rhabdomyosarcoma cells with and without exposure to IR. For colony formation assays, rhabdomyosarcoma cells were seeded in 12-well plates (approximately 1,250–10,000 cells/well for cells receiving radiation and 300–600 cells/well for cells receiving no treatment). After 24 hours, cells were subjected to varying degrees of radiation (2–8 Gy). Incubation time for colony formation assays between cell lines varied from 3 to 6 weeks. When colonies were sufficiently large, media was gently removed from each plate by aspiration, and colonies were fixed with 50% methanol for 10 to 15 minutes at room temperature. Colonies were then stained with 3% (w/v) crystal violet in 25% methanol for 10 to 15 minutes at room temperature, and excess crystal violet was washed with dH₂O with plates being allowed to dry. Colony formation was analyzed using ImageJ (Fiji). Significance was calculated by one-way ANOVA with Dunnett multiple comparisons tests. All assays were performed in triplicates.

Western blot analysis

Total cell lysates from human rhabdomyosarcoma cell lines and human myoblasts were obtained following lysis in RIPA lysis buffer supplemented with protease inhibitors (Roche). Western blot analysis was performed similar to Ignatius and colleagues, 2017 (27). Membranes were developed using an enhanced chemiluminescence (ECL) reagent (Western Lightning Plus ECL, PerkinElmer; or sensitive SuperSignal West Femto Maximum Sensitivity Substrate, Thermo Scientific). Membranes were stripped, rinsed, and reprobed with the respective internal control antibodies. List of primary and secondary antibodies is included in supplementary data (Supplementary Table S1). Western blots were quantified using ImageJ software, normalizing proteins of interest to their respective β -tubulin expression and the control [either skeletal human myoblast cells (hSKMC) or Scr of the same time point]. If control expression was zero, quantifications shown are shown as a ratio of the protein of interest expression to its respective β -tubulin expression.

IHC

Once tumors reached 4X the initial volume, mice were euthanized and tumors were fixed with 4% paraformaldehyde/PBS, sectioned, blocked, and stained with hematoxylin and eosin (H&E), Ki67, Myogenin (MYOG), and MF20 antibodies (see Supplementary Table S1).

Caspase-Glo 3/7 assay

Rh18, Rh30, and RD Scr- and SNAI2-knockdown cells were seeded at 20% confluency in 24-well plates and placed in the Incucyte ZOOM instrument. After reaching approximately 40% confluency, media was supplemented with Caspase-Glo 3/7 reagent (1:1,000, Essen Bioscience) and Nuclight reagent (1:500, Essen Bioscience). Cells were then subjected to a range of doses of IR (0 Gy–15 Gy) and placed back in the Incucyte. Images taken at 48 hours and 72 hours were processed using Adobe Photoshop and analyzed using ImageJ Cell Counter to determine percent caspase-3/7 events. Significance was determined using a two-way ANOVA with Sidak multiple comparisons test or one-way ANOVA with a *post hoc* Tukey test accordingly.

Flow cytometry

Rh18, Rh30, and RD Scr- and SNAI2-knockdown cells were seeded in 6-well plates and irradiated (PXi Precision X-Ray X-RAD 320). Cells were collected at varying time points (48, 72, 96, and 120 hours). A negative control of cells that did not receive IR were collected as well. Cells were centrifuged and resuspended in Annexin-binding buffer. After determining cell density and diluting to 1×10^6 cells/mL with Annexin-binding buffer, Annexin V conjugate, and propidium iodide were added to sample aliquots and left to incubate at room temperature in the dark for

15 minutes. After incubation, aliquots were mixed gently while adding Annexin-binding buffer on ice and analyzed by flow cytometry (LSRFortessa X-20; BD Biosciences). Cell cycle was assessed using the same cells and conditions described above with Click-iT EdU Alexa Fluor 647 Flow Cytometry Assay (ThermoFisher) according to the provided protocol. Significance was determined using a Two-Proportion Z-test.

RNA sequencing

RNA was extracted using the RNeasy mini kit (Qiagen). Poly-A-selected RNA libraries were prepared and sequenced on an Illumina HiSeq2000. Quality control was performed using FastQC version 0.11.2 and Picard version 1.127 RNASeqMetrics function with the default parameters. PCR duplicates were marked using Picard MarkDuplicates function. RNA sequencing (RNA-seq) reads were aligned to the University of California, Santa Cruz hg19 reference genome using TopHat version 2.0.13. Significance was defined as having FDR q value < 0.01 and family-wise error rate P value of < 0.05 . Gene set enrichment analysis (GSEA; <http://www.broadinstitute.org/gsea/index.jsp>) was performed using default parameter settings.

Chromatin immunoprecipitation sequencing and chromatin immunoprecipitation qPCR

Chromatin immunoprecipitation sequencing (ChIP-seq) data used, was published previously (28) and performed as follows. 1% Formaldehyde-fixed chromatin from RD and SMS-CTR cells were sheared to 200 to 700 bp with Active Motif EpiShear Sonicator. Chromatin immunoprecipitation (ChIP) with SNAI2 Ab (CST, catalog no. 9585) was performed overnight, using ChIP-IT High Sensitivity kit (Active Motif). Drosophila chromatin (Active Motif, catalog no. 53083) and H2Av ab (Active Motif, catalog no. #61686) was used for spike-in normalization across samples. ChIP-seq libraries were prepared using Illumina TruSeq ChIP Library Prep Kit and sequenced on NextSeq500. Reads were mapped to reference genome (version hg19) using Burrows–Wheeler Aligner (BWA). High-confidence ChIP-seq peaks were called by MACS2.1. Raw sequencing data and processed files are available through Gene Expression Omnibus (GEO; GSE137168). For qRT-PCR immunoprecipitated DNA was amplified with *BCL2L1* ChIP primers (SNAI2-binding peak 1 & 2) along with negative controls. All signals were normalized against input by the percentage input method. Significance was calculated by Unpaired t test.

Gene expression analysis

qRT-PCR was completed using the QuantStudio 7 Flex system (Applied Biosciences). PCR primers are provided in Supplementary Table S2 (28). RNA isolation and cDNA preparation were performed as previously described (27, 28). Significance was calculated by a two-way ANOVA with a Sidak multiple comparisons test. RNA-seq data, which includes alternative splice variants from Shern and colleagues (21) was used for correlation analyses. Noncoding- and nonsense-mediated decay isoforms were excluded from the analyses. Pairwise Pearson correlation of gene expression was calculated using R (version 4.0.5).

Results

SNAI2 expression directly correlates with protection from radiation in rhabdomyosarcoma cells

To better understand the factors regulating sensitivity to IR in rhabdomyosarcoma tumors, we used a panel of 8 representative human rhabdomyosarcoma cell lines namely JR1, RD, Rh18, Rh28, Rh30, Rh36, Rh41, and SMS-CTR. These cell lines include both embryonal rhabdomyosarcoma (ERMS) and alveolar rhabdomyosarcoma (ARMS) subtypes in which *TP53* is both mutant and WT

(Supplementary Table S3). Using an imaging-based platform to test different doses of IR on cell number/confluence, we found that Rh18, JR1, Rh28, and Rh41 cells are relatively more sensitive to IR while RD, SMS-CTR, Rh36, and Rh30 are more radioresistant (Fig. 1A–H; Supplementary Fig. S1A and S1B). Since *SNAI2* is known to protect cells from IR (9, 10), we analyzed *SNAI2* expression levels across rhabdomyosarcoma cell lines. Interestingly, the expression of *SNAI2* was correlated with the degree of protection from radiation, with Rh18, JR1, Rh28, and Rh41 showing low *SNAI2* expression levels while RD, SMS-CTR, Rh36, and Rh30 show relatively high levels of *SNAI2* protein. In contrast, the expression of proteins known to be involved post IR including *SNAI1*, *TWIST1*, *ZEB1*, *CHEK1*, and *CHEK2* were not correlated with radiosensitivity (Fig. 1I; Supplementary Fig. S2A). Analysis of *SNAI2* expression across rhabdomyosarcoma tumors and

cell lines indicates high *SNAI2* expression with a trend toward higher *SNAI2* expression in ERMS tumors compared with ARMS, but that expression is variable across tumors (Fig. 1J; ref. 28). Finally, analysis of the St. Jude PeCan Data Portal and The Cancer Genome Atlas (TCGA) for *SNAI2* expression showed that sarcomas, including rhabdomyosarcoma, are among the cancers that express the highest levels of *SNAI2* and have higher expression levels compared with control tissue (Fig. 1J; Supplementary Fig. S2B and S2C). These results suggest that *SNAI2* may have a protumorigenic function in rhabdomyosarcoma.

SNAI2 protects rhabdomyosarcoma cells from IR *in vitro*

To assess whether *SNAI2* protects rhabdomyosarcoma cells from IR, we performed *SNAI2*-knockdown experiments using validated

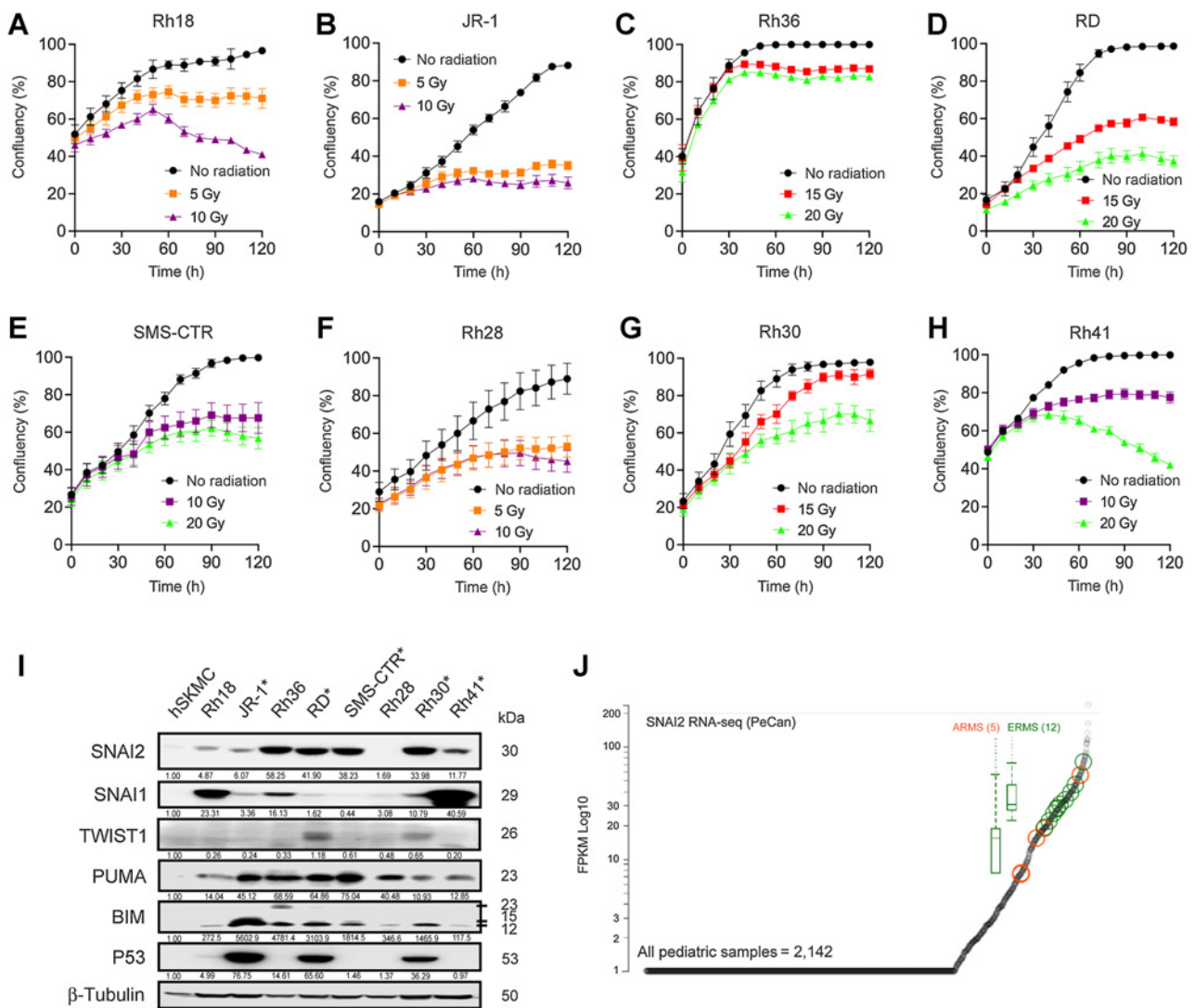


Figure 1. *SNAI2* expression directly correlates with radiosensitivity in rhabdomyosarcoma cells. **A–H**, Rh18, JR-1, Rh36, RD, SMS-CTR, Rh28, Rh30, and Rh41 cells were radiated at 24 hours post imaging with varying levels of radiation and cell confluency (%) was assessed using Incucyte Zoom software based on phase-contrast images acquired from 0 to 120 hours. Error bars, ± 1 SD. **I**, Western blot showing protein levels of *SNAI2*, *SNAI1*, *TWIST1*, *PUMA*, *BIM*, and *P53* in parental rhabdomyosarcoma (RMS) cell lines, with hSKMCs as a control. Asterisks (*) denote rhabdomyosarcoma cell lines with known *P53* mutations. **J**, PeCan *SNAI2* RNA-seq data for ARMS (orange) and ERMS (green) tumors.

Downloaded from http://aacrjournals.org/cancerres/article-pdf/81/21/5454/3085100/5454_1.pdf by guest on 13 January 2023

shRNAs in Rh30, RD, and Rh18 cells (25), which were chosen as representative lines with low, moderate, and high levels of radio-sensitivity (Fig. 1A–H; Fig. 2A–L). Compared with the Scr shRNA, two SNAI2 shRNAs (sh1 and sh2) reduced SNAI2 protein expression by 51% to 86% in Rh30, RD, and Rh18 cells (Fig. 2A, E, and I). Interestingly, while transient SNAI2 knockdown initially slowed cell proliferation (28), this effect was no longer observed once stable lines were generated (Fig. 2B, F and J). Each cell line was then exposed to an appropriate dose of IR (see Fig. 1A–H) and analyzed for confluency every 4 hours for 5 days (Fig. 2B, F and J). Compared with control-knockdown cells at 120 hours, SNAI2-knockdown cells became sensitized to IR across all 3 cell lines (Fig. 2C, G, and K). Similar results were observed in clonogenic colony-forming assays, where the surviving fraction of colonies was assessed in rhabdomyosarcoma cells exposed to a range of IR doses between 2 and 8 Gy. At lower doses of IR exposure, differences in

survival and colony formation were minimal compared with higher doses of IR where there was a clear separation between the shScr- and shSNAI2-treated cells (Fig. 2D, H, and L; Supplementary Fig. S3A). Next, to test whether overexpression of SNAI2 could promote radioresistance, we transfected control pBabe vector and SNAI2-Flag constructs into the highly radiosensitive Rh18 cell line and tested the response to IR (Supplementary Fig. S3B–S3D). While SNAI2 overexpression in Rh18 cells had no effect on proliferation in the absence of IR (Supplementary Fig. S3C), the cells became less sensitive to 10 Gy IR at 120 hours (Supplementary Fig. S3D). Since in SNAI2 knockdown rhabdomyosarcoma cells SNAI1 is induced and some rhabdomyosarcoma cells express high SNAI1, we assessed the effect of loss of SNAI1 on sensitivity to radiation in Rh18, RD, and Rh30 cells and show that SNAI1 ablated cells have similar survival to control cells post IR (Supplementary Fig. S3E–S3G). Thus, SNAI2 protects rhabdomyosarcoma cells from IR *in vitro*.

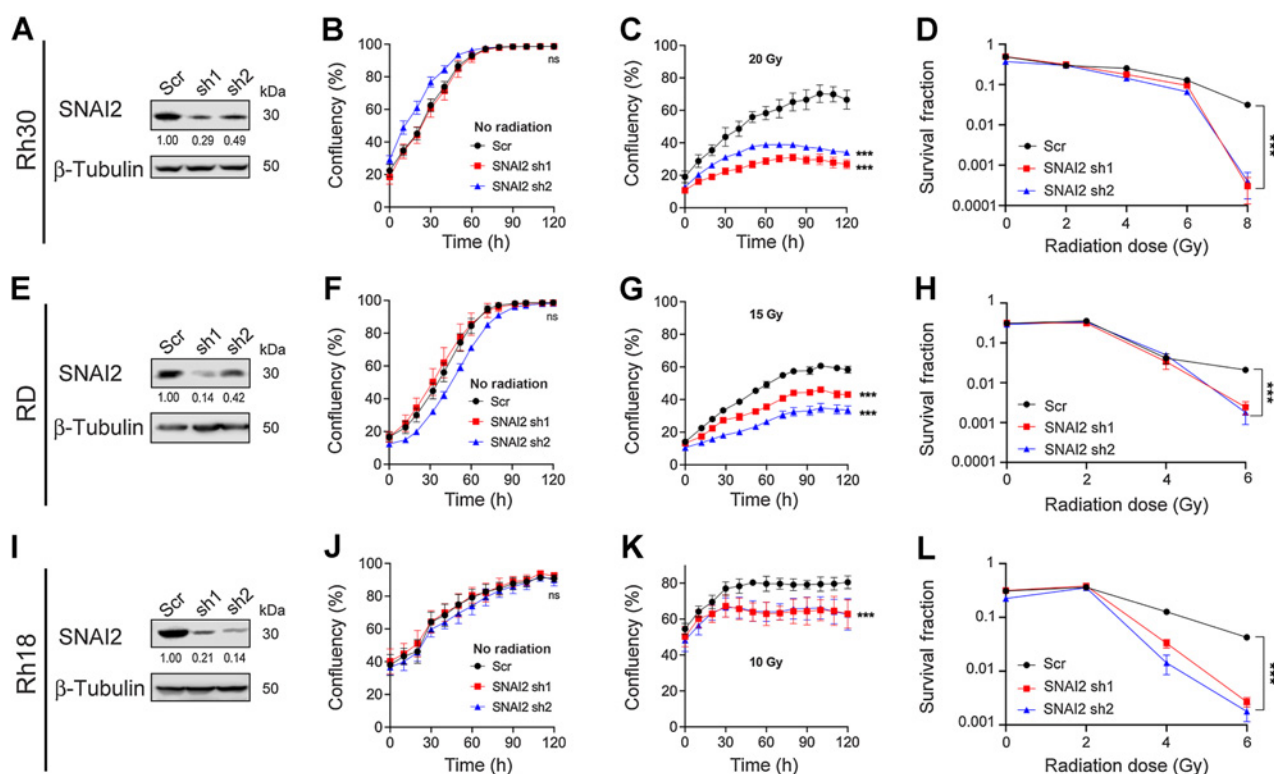


Figure 2.

SNAI2 protects rhabdomyosarcoma cells from IR *in vitro*. **A**, Western blot showing protein expression for SNAI2 of control (Scr shRNA) or SNAI2 knockdown (sh1 or sh2) in Rh30 cells. **B** and **C**, Cell confluency measured as a percent of the total of Rh30 cells with no IR or IR at 20 Grays (Gy) with either control or SNAI2 knockdown was assessed using phase-contrast images acquired from 0 to 120 hours. Error bars, ± 1 SD. ns, not significant; ****, $P < 0.0001$ by two-way ANOVA with Sidak multiple comparisons test. **D**, Survival fractions of Rh30 Scr and SNAI2-knockdown colony formation assays were assessed at increasing IR dose exposures. Error bars, ± 1 SD. Statistical differences were observed at 8 Gy. ****, $P < 0.0001$ by one-way ANOVA with Dunnett multiple comparisons test. **E**, Western blots showing protein expression for SNAI2 after control (Scr) or SNAI2 knockdown (sh1 or sh2) in RD cells. **F** and **G**, Cell confluency measured as a percent of the total of RD cells with no IR or IR at 15 Gy with either control or SNAI2 knockdown was assessed using phase-contrast images acquired from 0 to 120 hours. Error bars, ± 1 SD. ****, $P < 0.0001$ by two-way ANOVA with Sidak multiple comparisons test. **H**, Survival fractions of RD Scr and SNAI2-knockdown colony formation assays were assessed at increasing IR dose exposures. Error bars, ± 1 SD. Statistical differences were observed at 6 Gy. ****, $P < 0.0001$ by one-way ANOVA with Dunnett multiple comparisons test. **I**, Western blot showing protein expression of SNAI2 in control (Scr) or SNAI2 knockdown (sh1 or sh2) Rh18 cells. **J** and **K**, Cell confluency measured as a percent of the total of Rh18 cells with no IR or IR at 10 Gy in either control or SNAI2-knockdown cells was assessed using phase-contrast images acquired from 0 to 120 hours. Error bars, ± 1 SD. ****, $P < 0.0001$ by two-way ANOVA with Sidak multiple comparisons test. **L**, Survival fractions of Rh18 Scr and SNAI2-knockdown colony formation assays were assessed at increasing IR dose exposures. Error bars, ± 1 SD. Statistical differences were observed at 6 Gy. ****, $P < 0.0001$ by one-way ANOVA with Dunnett multiple comparisons test.

SNAI2 protects rhabdomyosarcoma tumors from IR *in vivo*

We next questioned whether SNAI2 could protect rhabdomyosarcoma tumor cells from IR *in vivo*. We created murine xenografts of Rh30 and Rh18 cells with SNAI2 knockdown and Rh18 cells with SNAI2 overexpression, as well as appropriate controls, and performed irradiation experiments after each group of mice developed palpable tumors (200–400 mm³). Rh30 and Rh18 tumors with SNAI2 (or control) knockdown were subjected to a cumulative 30-Gy dose of IR (2 Gy/day, 5 days per week, for 3 weeks). Following the completion

of the IR regimen, tumors were analyzed weekly for relapse (Fig. 3A–N). Relapse was defined by regrowth of tumors to 4 times their size prior to IR treatment (29). In the absence of IR, there were no significant differences in the growth rates between xenografts derived from Rh30 control- and SNAI2-knockdown cells (1 × 10⁶ cells injected/mouse, Fig. 3A; Supplementary Fig. S4A, n = 5). However, control Rh30 xenografts that were exposed to IR gave rise to relapse tumors significantly earlier (5 weeks post IR) than SNAI2-knockdown Rh30 xenografts (11–14 weeks post IR; Fig. 3A, Supplementary

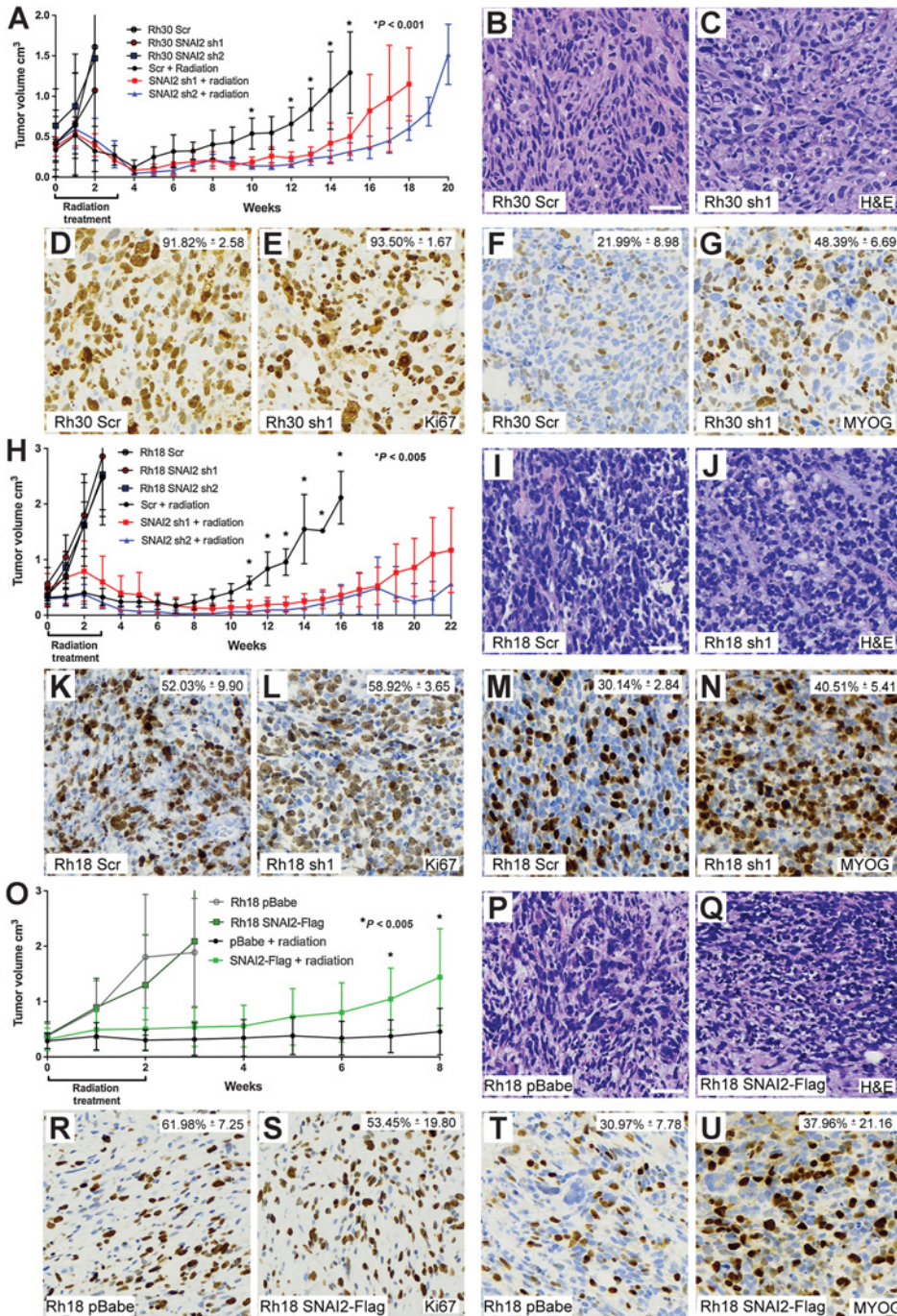


Figure 3. SNAI2 protects rhabdomyosarcoma tumors from IR *in vivo*. **A**, Growth curves of Rh30 xenografts including Scr shRNA and SNAI2 shRNA 1 and 2 (sh1, sh2) engrafted in mice. Xenograft growth was assessed under no IR and 30 Gy IR treatments. IR was given for 3 weeks at 2 Gy/day, 5 days a week. Error bars, ±1 SD. *, *P* < 0.001 by Student *t* test. **B** and **C**, H&E staining showing histology of Rh30 Scr and SNAI2-knockdown tumor sections. Scale bar, 100 μm. **D–G**, IHC analysis of Ki67 (**D** and **E**) staining to assess proliferation and MYOG staining (**F** and **G**) in Rh30 xenografts with either Scr shRNA or SNAI2 sh1. Ki67 – Scr versus sh1p. MYOG – Rh30 Scr versus Rh30 sh1. *P* < 0.05 by Welch *t* test. Magnification same as **B** and **C**. **H**, Growth curves of Rh18 xenografts including Rh18 Scr shRNA and SNAI2 shRNA 1 and 2 (sh1, sh2) engrafted in mice. Xenograft growth was assessed under no IR and 30 Gy IR treatments. IR was given for 3 weeks at 2 Gy/day for 5 days a week. Error bars, ±1 SD. *, *P* < 0.005 by Student *t* test. **I** and **J**, H&E staining showing histology of Rh18 Scr and SNAI2-knockdown tumor sections. Scale bar, 100 μm. **K–N**, IHC analysis of Ki67 (**K** and **L**) staining to assess proliferation and MYOG staining (**M** and **N**) in Rh18 xenografts with either Scr shRNA or SNAI2 sh1. MYOG – Scr versus sh1. *P* = 0.0519 by Welch *t* test. Magnification same as **I** and **J**. **O**, Growth curves of Rh18 xenografts expressing control vector (pBabe) and SNAI2-Flag engrafted in mice. Xenograft growth was assessed under no IR and 20 Gy IR treatments. IR was given for 2 weeks at 2 Gy/day for 5 days a week. Error bars, ±1 SD. *, *P* < 0.005 by Student *t* test. **P** and **Q**, H&E staining showing histology of Rh18 pBabe and SNAI2-Flag tumor sections. Scale bar, 100 μm. **R–U**, IHC analysis of Ki67 (**R** and **S**) staining to assess proliferation and MYOG staining (**T** and **U**) in Rh18 xenografts with either pBabe or SNAI2-Flag expression. Ki67 – pBabe versus SNAI2-Flag not significantly different. MYOG – pBabe versus SNAI2-Flag. *P* = 0.0519 by Welch *t* test. Magnification same as **P** and **Q**.

Downloaded from <http://aacrjournals.org/cancerres/article-pdf/81/21/5451/3085100/5451.pdf> by guest on 13 January 2023

Fig. S4B, $n = 8-10$). Similar to Rh30 xenografts, there were no differences in the growth rates between xenograft tumors derived from Rh18 control- and *SNAI2*-knockdown cells (5×10^6 cells injected/mouse) in the absence of IR (Fig. 3H; Supplementary Fig. S4C), and post IR control Rh18 xenografts gave rise to relapsed tumors significantly earlier (7 weeks post IR) than *SNAI2*-knockdown Rh18 xenografts (13–14 weeks post IR; Fig. 3H; Supplementary Fig. S4D, $n = 8-10$). Importantly, a subset of Rh18 *SNAI2* shRNA-knockdown tumors did not relapse until approximately 21 weeks post IR. Finally, Rh18 xenografts (5×10^6 cells injected/mouse) with control or *SNAI2* overexpression showed no differences in growth rate in the absence of IR (Fig. 3O–U; Supplementary Fig. S4E, $n = 4$), but following a cumulative 20-Gy dose of IR (2 Gy/day, 5 days per week, for 2 weeks), *SNAI2*-overexpressing Rh18 xenografts relapsed more rapidly than control Rh18 xenografts (Fig. 3O; Supplementary Fig. S4F, $n = 8-9$).

To investigate the effect of *SNAI2* knockdown on tumor histology, proliferation, and differentiation in Rh30 and Rh18 relapsed tumors, xenografts with Scrambled or *SNAI2* knockdown were harvested from mice once they reached 4X their initial volume and tumors were processed, sectioned, and assessed for histology (H&E), proliferation (Ki67), and differentiation (MYOG). H&E analysis did not show significant differences between Scrambled versus *SNAI2* knockdown tumors (Fig. 3B, C, I, and J). Next, Ki67 staining showed Control (shScr) and *SNAI2* knockdown xenografts proliferate at similar rates (Fig. 3D, E, K, and L). In Rh30 and Rh18 tumors with *SNAI2* shRNA knockdown, there was a trend toward areas showing increased MYOG expression (Fig. 3F, G, M, and N). However, this increase in MYOG did not result in terminal differentiation as assessed by MyHC (MF20) staining (Supplementary Fig. S4G–S4J). Similarly, there was not a significant effect on tumor histology, proliferation, or differentiation observed when comparing Rh18 controls with Rh18 *SNAI2*-overexpressing xenografts (Fig. 3P–U). Thus, while the H&E and MYOG staining showed that *SNAI2* may also inhibit myogenic differentiation in some rhabdomyosarcoma tumors; however, this effect is not as prominent compared with our previously described results in RAS-mutant ERMS (28). Altogether, our data suggest that the major conserved effect of *SNAI2* post IR is to protect rhabdomyosarcoma tumors from IR *in vivo*.

Loss of *SNAI2* promotes IR-mediated apoptosis and blocks irradiated rhabdomyosarcoma cells from exiting the cell cycle

To better understand how *SNAI2* protects rhabdomyosarcoma cells from IR, we assessed the effects of *SNAI2* knockdown on apoptosis and the cell cycle in rhabdomyosarcoma cell lines. We first analyzed live cells for signs of apoptosis using a Caspase-Glo assay in Rh30, RD, and Rh18 cells. In the absence of IR, control- and *SNAI2*-knockdown cells grew at similar rates (see Fig. 2B, F, and J) and had significantly lower caspase-3/7 staining until they reached confluence in all 3 rhabdomyosarcoma cell lines (Supplementary Fig. S5A). However, at 72 hours post IR (hpIR), *SNAI2*-knockdown cells exhibited a significant increase in apoptosis compared with controls (Fig. 4A–C; Supplementary Fig. S5B). We then performed independent apoptosis assays using Annexin V/propidium iodide staining to confirm these findings by analyzing live cells post IR by flow cytometry. Consistent with the Caspase-Glo assay, there was a significant increase in early- and late- apoptotic cells in the *SNAI2*-knockdown Rh30, RD, and Rh18 populations between 72 to 120 hpIR compared with control-knockdown cells (Fig. 4D–G; Supplementary Fig. S5C and S5D). Importantly, in the absence of IR, there were no significant differences in apoptosis between control-

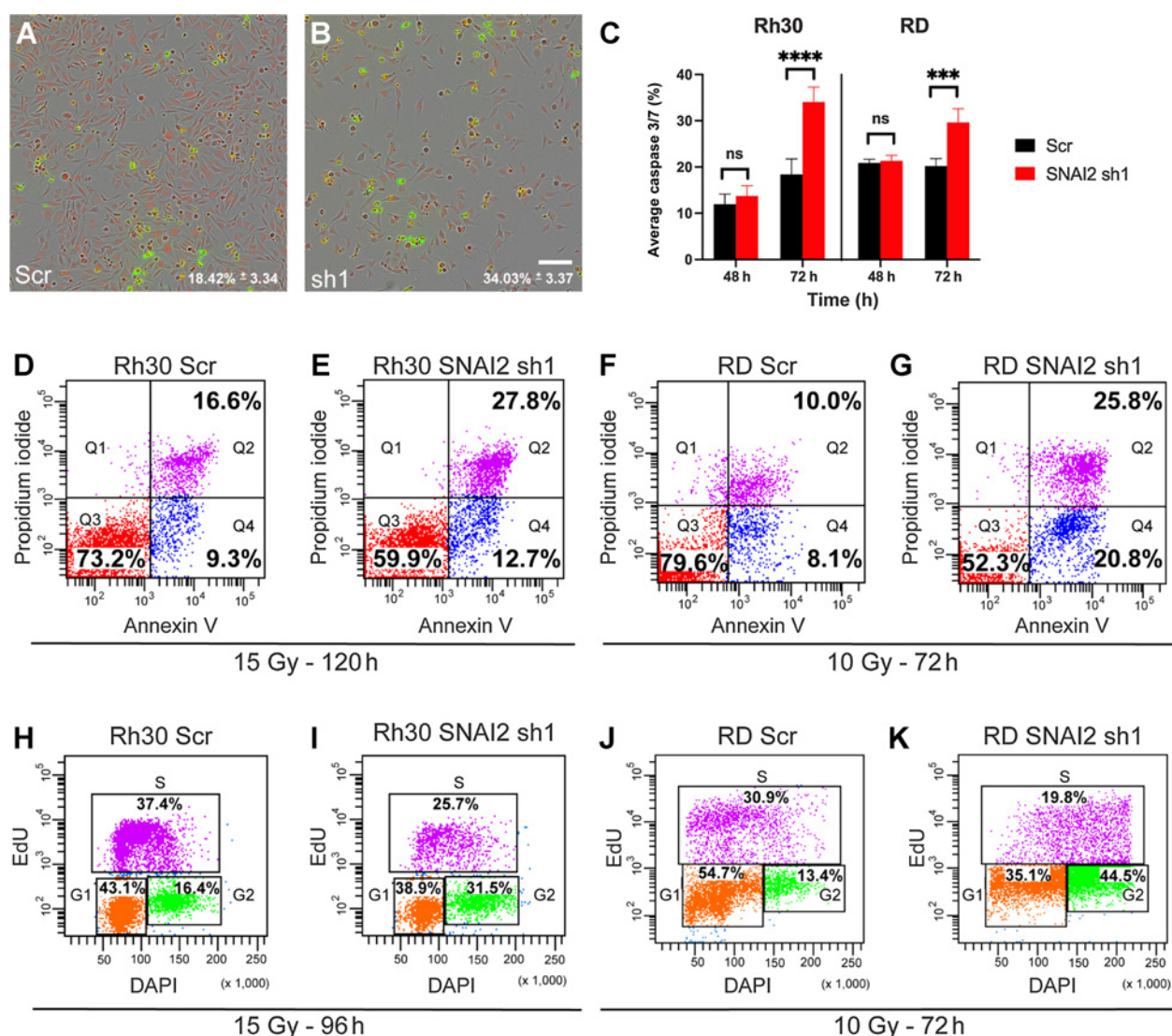
and *SNAI2*-knockdown cells for each of the cell lines (Supplementary Fig. S5E–S5J). These experiments indicate that *SNAI2* protects rhabdomyosarcoma cells from IR-induced apoptosis.

We next analyzed whether *SNAI2* regulates the cell cycle after exposure to IR using EdU labeling followed by flow cytometry. Following IR treatment, *SNAI2*-knockdown cells showed a significant reduction in cells in the G₁ and S phases and an accumulation of cells in the G₂-M phase of the cell cycle, indicative of a G₂-M block (Fig. 4H–K; Supplementary Fig. S5K and S5L). In the absence of IR, there were no differences in proliferation between control- and *SNAI2*-knockdown cells (Supplementary Fig. S5M–S5R). These experiments suggest that loss of *SNAI2* may prevent mitosis or alter progression through the M-phase of the cell cycle following exposure to IR.

SNAI2 represses the expression of the BH3-only BIM in rhabdomyosarcoma cells

To investigate the mechanisms by which *SNAI2* protects rhabdomyosarcoma cells from IR-induced apoptosis, we analyzed the expression of both pro- and antiapoptotic regulators of mitochondrial apoptosis across rhabdomyosarcoma cells (Supplementary Fig. S2C) and more specifically in Rh30, RD, and Rh18 cells expressing shScr versus sh*SNAI2* with and without IR (Fig. 5A and B; Supplementary Fig. S6A). In response to IR, *SNAI2*-knockdown cells showed increased expression of the apoptosis-marker cleaved-PARP, which is prominent especially between 72 to 96 hpIR and consistent with the Annexin V and Caspase-Glo analyses (Fig. 4D–G; Supplementary Fig. S5C and S5D). In the absence of IR, expression of the proapoptotic BH3-only regulator PUMA/BBC3 appears to be upregulated upon *SNAI2* knockdown in all cell lines. Interestingly, *SNAI2* knockdown also elicited a prominent increase in the proapoptotic BH3-only BIM across all 3 cell lines as well as in BID and BAX in Rh18 and BID in Rh30 lines. With respect to antiapoptotic regulators, BCL2 showed a modest increase in both Rh30 and Rh18 in response to *SNAI2* knockdown in the absence of IR, while BCL_{-XL} expression was elevated in RD and Rh30. Moreover, in response to IR treatment, BCL2, MCL1, and BCL_{-XL} varied across cell lines and failed to correlate with *SNAI2* knockdown. Among the regulators of apoptosis, only BIM expression was found to be consistently elevated across all cell lines in response to *SNAI2* knockdown in IR-exposed cells. These experiments indicate that *SNAI2*, in addition to its known function as a transcriptional repressor of PUMA (10, 30), appears to repress the expression of BIM in rhabdomyosarcoma cells.

To determine the mechanism by which *SNAI2* influences the cell cycle in rhabdomyosarcoma cells, we analyzed the expression of the P21/CDKN1A cell-cycle checkpoint inhibitor and found that *SNAI2* knockdown leads to upregulation of P21 in both Rh30 and RD cells (Fig. 5C). Since P21 is also a marker of cells undergoing senescence, we analyzed P16 expression and performed β -gal staining in Rh30 and RD cells. There were no differences in P16 expression or β -gal staining between control and *SNAI2* knockdown in either cell type, suggesting that senescence is not regulated by *SNAI2* in these cells (Fig. 5C; Supplementary Fig. S6B–S6E). In rhabdomyosarcoma tumors, CDKN1A/P21 expression is often repressed, and reexpression of P21 promotes differentiation (31, 32). Moreover, *SNAI2* has been shown by ChIP-seq experiments to indirectly block *CDKN1A* expression in ERMS RD and SMS-CTR cells, and co-knockdown of *CDKN1A* and *SNAI2* in RD and JR1 rhabdomyosarcoma cells results in the loss of differentiation-positive, myosin heavy-chain-expressing cells (28). We also assayed the effect of *SNAI2* knockdown on differentiation post IR in Rh30 and RD cells and in another ERMS cell line with WT P53, Rh36. Both RD and Rh36 are RAS-mutant ERMS cell lines. Following exposure to IR, RD and Rh36 cells with *SNAI2* knockdown exhibited a

**Figure 4.**

Loss of SNAI2 promotes IR-mediated apoptosis and blocks irradiated rhabdomyosarcoma cells from exiting the cell cycle. **A** and **B**, Representative images of Caspase-Glo assay in Rh30 cells (either control or SNAI2 knockdown) at 72 hours post IR exposure (15 Gy) with red-labeling cells/nuclei and green-labeling caspase-3/7; average caspase-3/7 levels (%) were quantified in **C**. Scale bar, 150 μ m. **C**, Average caspase-3/7 percentage (mean \pm 1 SD) in Rh30 and RD Scr and SNAI2 sh1 cells 48 hours and 72 hours after IR exposure of 15 or 10 Gy, respectively. ***, $P < 0.001$; ****, $P < 0.0001$ by two-way ANOVA with Sidak multiple comparison. **D–G**, Flow cytometry plots showing propidium iodide versus Annexin V staining of Rh30 and RD Scr or SNAI2 sh1 cells and treated with indicated IR doses. Q4 represents cells undergoing early apoptosis, whereas Q2 represents cells undergoing late apoptosis. Q3 represents live cells not undergoing apoptosis. Rh30 early apoptosis (Q4): Scr 9.3% versus sh1 12.7%, $P < 0.0001$; late apoptosis (Q2): Scr 16.6% versus sh1 27.8%, $P < 0.0001$; RD early apoptosis (Q4): Scr 8.1% versus sh1 20.8%, $P < 0.0001$; late apoptosis (Q2): Scr 10.0% versus sh1 25.8%, $P < 0.0001$ by two-proportion Z test. **H–K**, Flow cytometry plots of EdU versus DAPI staining in Rh30 and RD cells with either Scr shRNA or SNAI2 sh1 after exposure to indicated IR doses. Rh30 Scr versus sh1 G₂ phase, $P < 0.0001$; RD Scr versus sh1 G₂ phase, $P < 0.0001$ by two-proportion Z test.

significant increase in differentiation as determined by the expression of differentiated myosin MF-20 staining (Supplementary Fig. S6F–S6K). In contrast, in Rh30 (ARMS) cells this effect was not as prominent (Supplementary Fig. S6L), suggesting that SNAI2 may be more important for the suppression of muscle differentiation in RAS-mutant ERMS tumors consistent with our previous findings (28).

We next questioned whether SNAI2 regulates IR-induced DNA repair. Since IR primarily causes DNA double-stranded breaks, we analyzed the expression of a well-established marker for these DNA

lesions, γ H2AX (33), during a time course following IR in Rh30 and RD cells via Western blot analysis (Fig. 5D). As expected, γ H2AX levels increased rapidly following exposure to IR in both cell lines with SNAI2-knockdown cells showing similar increases compared with control-knockdown cells; however, γ H2AX expression was retained as late as 48 hours in SNAI2-knockdown cells, suggesting a delay in the ability of SNAI2-knockdown cells to repair damaged DNA (Fig. 5D). However, SNAI2-knockdown RD and Rh30 cells have little if any differences in expression of DNA-damage checkpoint regulators

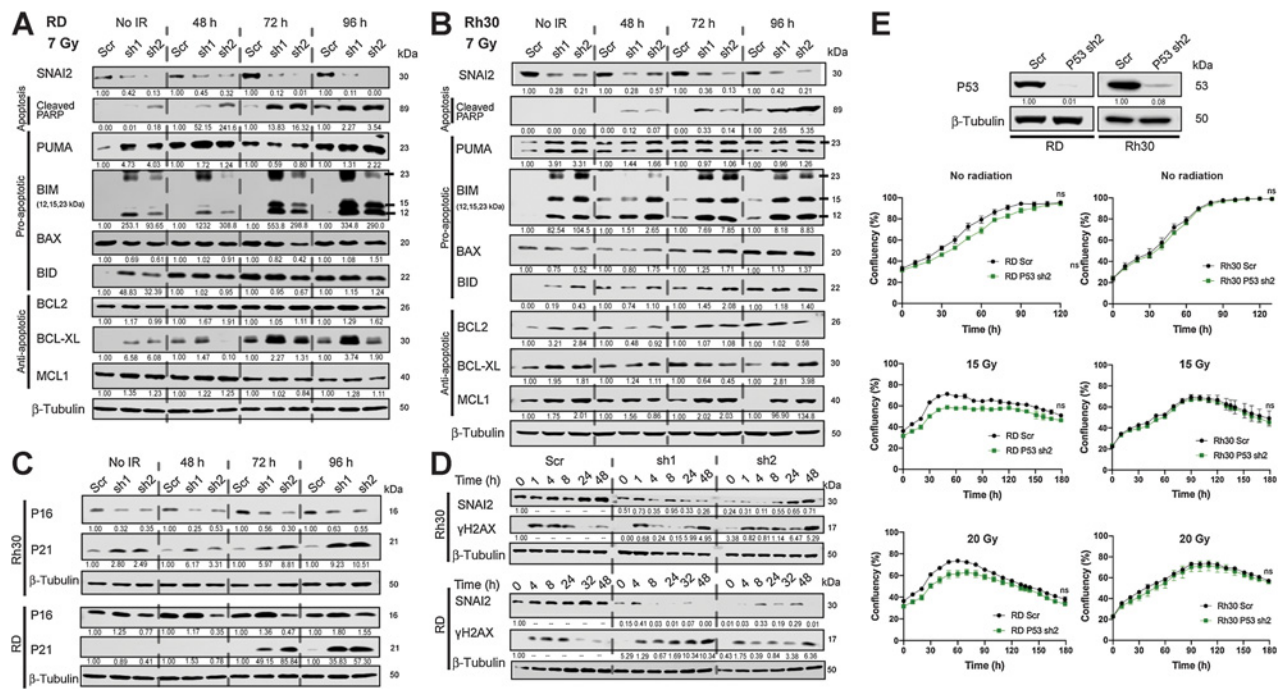


Figure 5. SNAI2 represses the expression of BH3-only BIM in rhabdomyosarcoma cells. **A** and **B**, Western blot analyses to determine protein expression of SNAI2, cleaved PARP, PUMA, BIM, BAX, BID, BCL2, BCL-XL, and MCL1 in RD and Rh30 cells under no IR or at 48, 72, or 96 hours post IR after 7 Gy treatment. **C**, Western blot analysis to determine protein expression of P16 and P21 in Rh30 and RD cells under no IR or at 48, 72, or 96 hours post IR with 7 Gy. Protein used for RD cell line Western blots was from the same analyses for experiments in **Fig. 5A**, therefore the β -tubulin blot is the same as in **A**. **D**, Western blot analysis of γ H2AX over time after exposure to 7 Gy IR in Rh30 and RD control (Scr) and SNAI2-knockdown (sh1 and sh2) cells. **E**, Western blot analysis to determine protein levels of P53 in RD and Rh30 cells (either Scr control or P53 sh2 knockdown). Confluency (%) of non-IR or IR-treated (15 or 20 Gy) RD and Rh30 cells (with either Scr control or P53 shRNA knockdown) was assessed on phase-contrast images acquired from 0 to 180 hours. No statistical differences were observed. Error bars, ± 1 SD. ns, not significant by unpaired *t* test.

pCHEK1 and pCHEK2 following IR (Supplementary Fig. S6M and S6N). These findings suggest that SNAI2 might have additional roles on influencing the timing of repair of DNA double-strand breaks in rhabdomyosarcoma cells.

Both Rh30 and RD cells have *TP53* mutations that aberrantly stabilize the P53 protein (Fig. 1E; refs. 34, 35). To determine if the expression of mutant P53 is important for IR-mediated inhibition of cell growth in RD and Rh30 cells, we performed an shRNA-mediated knockdown of P53 and tested its effects on the RD and Rh30 lines (Fig. 5E). In both lines, knockdown of mutant P53 failed to affect sensitivity to IR (Fig. 5E). Additionally, in both Rh30 and RD cells, SNAI2 is slightly induced or maintained following IR, suggesting alternate mechanisms by which SNAI2 expression is modulated in rhabdomyosarcoma (Fig. 5D).

Direct repression of *BIM* by SNAI2 blocks apoptosis in irradiated rhabdomyosarcoma cells

Since BIM was consistently and robustly induced by loss of SNAI2 in rhabdomyosarcoma cells and apoptosis post IR is the major effect of SNAI2 ablation across all rhabdomyosarcoma cells assessed, (Fig. 5A and B; Supplementary Fig. S6A) we questioned whether SNAI2 could directly repress expression of BH3 proapoptotic regulator *BIM*. We first performed RNA-seq analysis comparing control- and SNAI2-knockdown in RD cells at 24 hpIR (5 Gy). GSEA pathway analysis revealed that in addition to differences in myogenic differentiation, several stress-response pathways were modulated in response to IR.

These pathways included “hypoxia”, “UV response down”, and “apoptosis” (Fig. 6A). Several apoptotic pathway genes were increased or decreased in SNAI2-knockdown cells post IR (Fig. 6B). We performed qRT-PCR analysis using RD and Rh30 cells for a subset of the apoptotic regulators and validated the upregulation of *CDKN1A* (only RD), *BCL2L11*(*BIM*), and *DAP* and downregulation of *FDXR*, *F2R*, *PDGFRB*, *CLU*, *IER3*, and *TAP1* (Fig. 6C; Supplementary Fig. S7A). We also analyzed the correlation between *SNAI2* expression and *BIM/BCL2L11* and other pro- and antiapoptotic regulators in human rhabdomyosarcoma tumors and find that *SNAI2* expression is significantly negatively correlated with at least one alternatively spliced transcript coding for *BIM/BCL2L11* but not for *PUMA/BBC3* or *BMF* transcripts (Fig. 6D; Supplementary Tables S4 and S5). Finally, ChIP-seq analysis of SNAI2 binding in SMS-CTR and RD cells with shScr and shSNAI2-knockdown treatments was used to assess SNAI2-chromatin-binding peaks in BH3 containing proapoptotic regulators. Our analyses show that SNAI2 binds to enhancers associated with *BIM/BCL2L11* (Fig. 6E; ref. 28) and *BMF* (Supplementary Fig. S7B). In contrast, no SNAI2 shared binding peaks in SMS-CTR and RD cells were found associated with the promoter-enhancer regions of *CDKN1A* (Supplementary Fig. S7B; ref. 28), *PUMA/BBC3* or other pro- and antiapoptotic regulators (Supplementary Fig. S7B). To validate the ChIP-seq findings, we performed ChIP-qPCR analyses at the SNAI2-binding sites downstream of *BIM/BCL2L11* and confirmed that SNAI2 enrichment is relatively increased at the distal enhancer contained within the *BIM/BCL2L11* topologically

Downloaded from <http://aacrjournals.org/cancerres/article-pdf/81/21/5451/3085100/5451.pdf> by guest on 13 January 2023

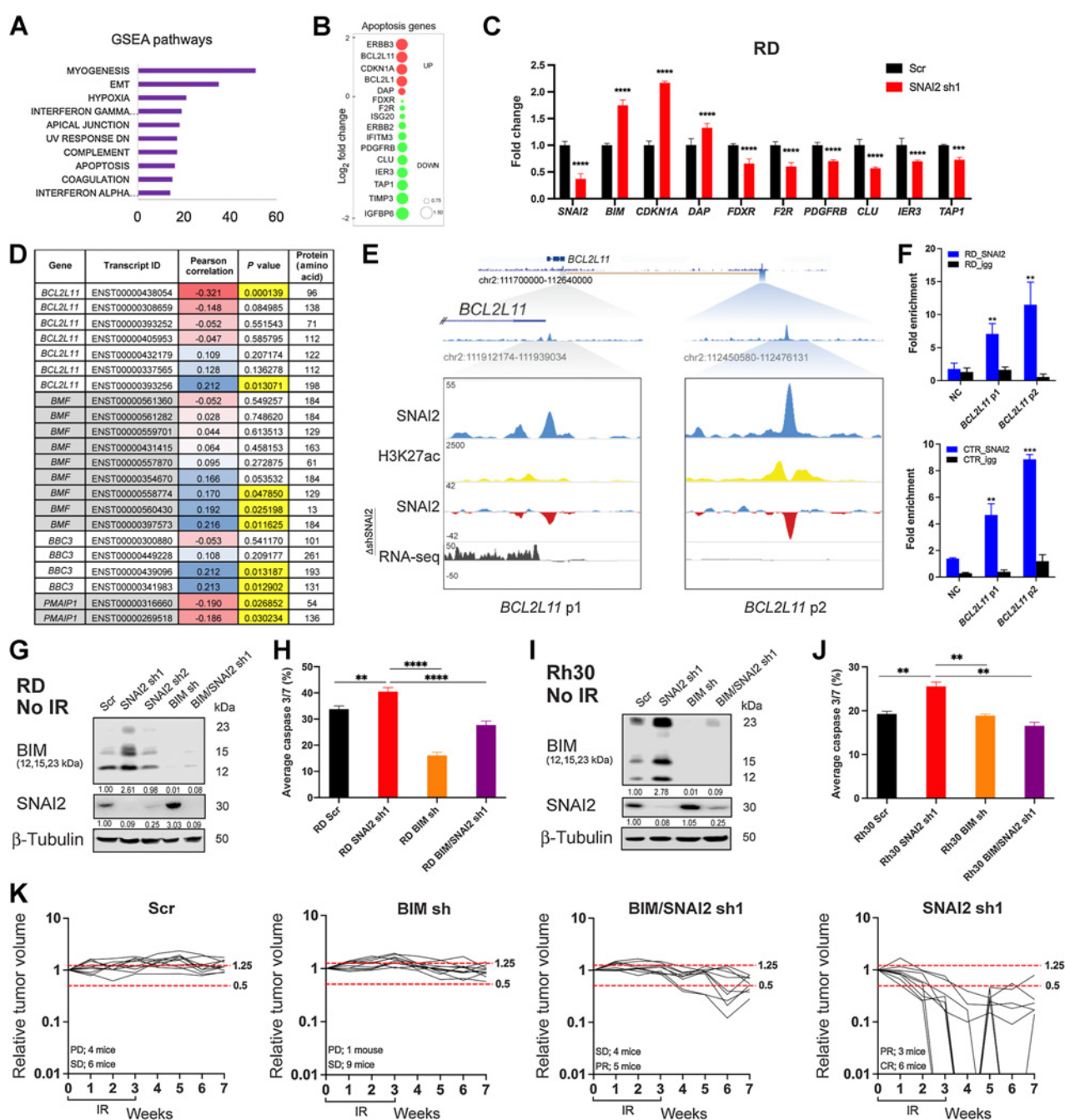


Figure 6.

Direct repression of *BIM* by *SNAI2* blocks apoptosis in irradiated rhabdomyosarcoma cells. **A**, GSEA pathway analysis comparing mRNA expression (RNA-seq) in control/Scr and *SNAI2* shRNA-treated RD cells 24 hours post IR (5 Gy). Enriched pathways in sh*SNAI2* cells (GSEA Hallmark pathways) with number of upregulated genes in each pathway class (x-axis). **B**, RNA-seq data showing genes highly upregulated or downregulated when comparing control/Scr- and *SNAI2*-shRNA knockdown RD cells 24 hours post IR (5 Gy). Red circles, upregulated genes; green circles, downregulated genes; size of circles, log₂-fold change compared with shScr. **C**, qRT-PCR analysis (mean \pm 1SD) of various cell-cycle and apoptosis genes in RD cells 48 hours after irradiation with 5 Gy. ***, $P < 0.001$; ****, $P < 0.0001$ by two-way ANOVA with a Sidak multiple comparisons test. **D**, Pearson correlation between the expression of *SNAI2* and proapoptotic regulators *BIM/BCL2L11*, *BMF*, *BBC3*, and *PMAIP1* in primary-human rhabdomyosarcoma assessed by RNA-seq analysis. Blue cells indicate positive correlation, while red cells indicate negative correlation. **E**, ChIP-seq tracks of *SNAI2* (blue), H3K27ac (yellow) binding at the *BIM/BCL2L11* locus in SMS-CTR cells in shScr cells and delta (Δ) enrichment value (sh*SNAI2* sh1 minus shScr, blue and red) for *SNAI2* and gene expression (RNA-seq, black). Boxed area corresponds to *SNAI2*-binding region and shaded areas represent relative position of the peaks to the TAD containing *BCL2L11*. Values on y-axis represent fold enrichment. **F**, ChIP-qPCR of *SNAI2*-enriched regions downstream of *BIM/BCL2L11* gene in RD and SMS-CTR cells. Fold enrichment value of *SNAI2* at the *BCL2L11*-peak1 and peak2 is plotted along with negative control (NC) region and IgG controls, **, $P < 0.01$; ***, $P < 0.0001$ by unpaired *t* test compared with negative control. **G**, Western blot analyses of *BIM* and *SNAI2* expression in non-IR-treated RD cells under either Scr control, *SNAI2* shRNA, *BIM* shRNA, or double *BIM/SNAI2* shRNA conditions. (Continued on the following page.)

associating domain (TAD; Fig. 6F; Supplementary Fig. S8) consistent with our ChIP-seq results. Together, these experiments establish that SNAI2 is a direct repressor of proapoptotic *BIM/BCL2L1*.

We next questioned whether reducing BIM expression would abrogate the SNAI2-knockdown-induced radiosensitivity in rhabdomyosarcoma cells. We therefore generated RD and Rh30 cells with stable lentiviral infections for (i) control shRNA, (ii) *SNAI2* shRNA, (iii) *BIM* shRNA, and (iv) both *SNAI2* and *BIM* shRNAs (Fig. 6G–K; ref. 26). Consistent with our earlier findings, knockdown of SNAI2 increased the levels of all three forms of BIM, which was reversed by concomitant knockdown of BIM (Fig. 6G and I). As expected, IR treatment of SNAI2-knockdown RD and Rh30 cells with a single dose of 15 Gy resulted in selective loss of confluency (Supplementary Fig. S9A and S9B) and a significant increase in caspase-3/7-positive cells compared with irradiated control-knockdown cells. However, this effect on apoptosis and confluency was significantly reversed in SNAI2/BIM double-knockdown cells post IR (Fig. 6H and J; Supplementary Fig. S9A and S9B). Of note, in the absence of IR, no differential effects on confluency or apoptosis were observed across all 4 groups (Supplementary Fig. S9C and S9D). Since the SNAI2/BIM-knockdown-mediated rescue of radiosensitivity in Rh30 cells was only partial, it is possible that other SNAI2-regulated genes may also contribute to IR-induced effects (Supplementary Fig. S9B). Finally, we tested in RD xenografts the effect of combined knockdown of SNAI2 and BIM on response to IR. We created murine xenografts of RD with shScr, shBIM, shSNAI2, and shSNAI2/BIM double-knockdown conditions. After each group of mice developed palpable tumors (200–400 mm³), they were subjected to a cumulative 30-Gy dose of IR (2 Gy/day, 5 days per week, for 3 weeks). Following the completion of the IR regimen, tumors were analyzed weekly for changes in tumor volume. While shScr and shBIM tumors showed no effect on relative change in tumor volume post IR compared with their initial volumes, with animals demonstrating either SD or PD, in the shSNAI2 group, 6 of 9 tumors showed a CR, while the other 3 of 9 showed a partial response PR 4 weeks post IR (Fig. 6K). In contrast, in the double SNAI2/BIM shRNA group none of the tumors resulted in a CR. Instead, only 5 of 9 tumors resulted in a PR, whereas the remaining 4 mice demonstrated SD. Indeed, the relative change in tumor volume post IR compared with their initial volumes in shSNAI2 xenografts were significantly decreased compared with double SNAI2/BIM-knockdown xenografts (Fig. 6K). Together, these experiments show that SNAI2-mediated repression of *BIM* protects rhabdomyosarcoma cells from the effects of IR.

Discussion

Radiation therapy is an important component of rhabdomyosarcoma treatment, especially during the management of metastases in patients at high-risk (2, 3, 5). Identifying pathways that regulate the response to IR therapy could potentially provide biomarkers of resistance or sensitivity to IR as well as targets for therapeutic intervention. Here, we show that SNAI2 directly represses the proapoptotic BH3-only gene *BIM* to protect rhabdomyosarcoma tumors from IR.

SNAI2 protects rhabdomyosarcoma tumor cells from IR despite the fact that the P53 pathway is nonfunctional or is mutant and consequently PUMA induction is not robust in the *TP53*-mutant rhabdomyosarcoma cell lines tested in this study. In lymphocytes and other highly radiosensitive cell types, P53 becomes rapidly activated in response to IR, and triggers mitochondrial apoptosis through induction of the expression of *PUMA* (10). Our finding that SNAI2 expression levels appear to dictate radiosensitivity of rhabdomyosarcoma cells in a manner that is independent of *TP53*-mutant status and possibly *PUMA* expression, but rather by direct repression of *BIM* that is not directly regulated by P53, suggests an important role for SNAI2 in the radiation response in cancer cells that can be dependent or independent of P53. Experiments *in vivo* in mice mutant for *Puma* and *Bim* demonstrate that both *Puma* and *Bim* can potently trigger the mitochondrial apoptosis response post radiation. Further, the loss of *Bim* protects lymphocytes from radiation and decreases the time to tumor initiation in thymocytes compared with wildtype controls (11, 36–38). This effect of BIM protecting cells from radiation is seen by correlation in renal cell carcinomas (RCC) and also in KRAS mutant lung-cancer cell lines. Correlation studies in RCCs that often have mutations in *VHL* express low levels of BIM (EL) and are more resistant to several apoptotic stimuli, including UV radiation (39). Also, in a subset of KRAS-mutant lung cancer cell lines, low BIM expression was associated with relative resistance to radiation (40). Thus, BIM is a bona fide BH3 proapoptotic regulator that can be induced post IR to mediate mitochondrial apoptosis. Our study shows that in rhabdomyosarcoma tumors, SNAI2 is a potent repressor of *BIM* expression, yet its expression can be independent of *TP53*. In support of this assertion, we have recently found in the ERMS subtype that both MEK signaling and muscle-specific regulator MYOD maintains SNAI2 expression; while in the ARMS subtype the PAX3-FOXO fusion oncogene is also known to be required for SNAI2 expression (28, 41, 42).

Despite the presence of different genetic drivers namely, the PAX3-FOXO fusion oncogene in ARMS lines and mutant RAS and amplified MDM2 in the ERMS lines among the cell lines used in this study, the radiosensitivity of each cell line correlated with expression of SNAI2 rather than oncogene/tumor-suppressor status. This suggests that SNAI2 expression levels could be used to predict the degree of radiosensitivity across different rhabdomyosarcoma tumors, and perhaps multiple tumor types. For example, most solid tumors have intermediate levels of SNAI2 and intermediate sensitivities to IR (Supplementary Fig. S1C; refs. 43, 44). In contrast, melanomas and osteosarcomas, which are generally not treated with IR in the clinic due to their inherent radioresistance and radiation when administered at high doses for local control of disease and in palliative care (45–47), have the highest levels of SNAI2 expression. This makes sense from a developmental perspective since sarcomas originate from mesoderm (48, 49), a tissue that expresses high levels of SNAI2 during development and has roles in muscle, bone, and cartilage tissues (reviewed in ref. 8). The analysis of SNAI2 expression levels could therefore be potentially informative for the treatment of multiple different cancers.

(Continued.) **H**, Average caspase-3/7 (%) (mean ± 1 SD) in RD Scr, SNAI2 sh1, BIM sh, and BIM/SNAI2 sh1 cells 72 hours after IR exposure (15 Gy). **, $P < 0.01$; ****, $P < 0.0001$ by one-way ANOVA with Tukey multiple comparisons test. **I**, Western blot analyses of BIM and SNAI2 expression in non-IR-treated Rh30 cells under either Scr control, SNAI2 shRNA, BIM shRNA, or double BIM/SNAI2 shRNA conditions. **J**, Average caspase-3/7 (%) (mean ± 1 SD) in Rh30 Scr, SNAI2 sh1, BIM sh, and BIM/SNAI2 sh1 cells 72 hours after IR exposure (15 Gy). **, $P < 0.01$ by one-way ANOVA with Tukey multiple comparisons test. **K**, Individual relative tumor volumes of RD Scr, SNAI2 sh1, BIM sh, and BIM/SNAI2 sh1 xenografts after 30 Gy (2 Gy/day, 5 × a week, for 3 weeks). Change in volume 2 weeks post IR: shScr = 0.0295 cm³/week, shBIM = 0.01125 cm³/week; no significant difference by one-way ANOVA with Tukey multiple comparisons test. Change in volume 2 weeks post IR: shSNAI2 = -0.067 cm³/week, shSNAI2/BIM = -0.0105 cm³/week; $P < 0.0001$ by one-way ANOVA with Tukey multiple comparisons test.

Rhabdomyosarcoma cells with stable SNAI2 knockdown while showing relatively little differences in proliferation, apoptosis, or cell viability compared with controls, nevertheless have consistent increased expression of proapoptotic modulators BIM, PUMA, and BID at baseline even in cells not exposed to IR. Additionally, our studies show that SNAI2 directly represses *BIM* expression. This suggests that SNAI2-knockdown cells are primed for mitochondrial apoptosis and an important oncogenic role for SNAI2 is to prevent IR-induced mitochondrial apoptosis. In contrast to the consistent expression of BIM and PUMA, in untreated cells different antiapoptotic regulators, *BCL2*, *BCL_{XL}*, and *MCL1*, are expressed at varying levels in the Rh30, RD, and Rh18 rhabdomyosarcoma lines to balance proapoptotic factor expression in SNAI2 knockdown cells. Additionally, we find relatively different protein levels of several pro- and antiapoptotic regulators across commonly studied rhabdomyosarcoma cell lines (Supplementary Fig. S2C). Based on these observations, one would predict that treating rhabdomyosarcoma cells with inhibitors of *BCL2*, *BCL_{XL}*, and *MCL1* in the context of SNAI2 knockdown would have variable effects on mitochondrial apoptosis and might be an important factor when considering combination treatments, whereas increasing BIM activity would further prime rhabdomyosarcoma tumors to undergo apoptosis.

In summary, our study implicates SNAI2 as a potential biomarker for IR sensitivity in rhabdomyosarcoma, with an inverse correlation between SNAI2 expression levels and radiosensitivity of the tumor cells. Post IR in conditions where SNAI2 expression is reduced, both ERMS and ARMS cell lines exhibit significantly reduced cell growth in addition to increased levels of apoptosis. ERMS cell lines may also undergo differentiation following exposure to IR. Differences in other known pathways that could explain reduced cell proliferation, such as senescence and dysfunctional DNA repair, were either variable or not observed in the SNAI2-knockdown cells compared with control rhabdomyosarcoma cells. Indeed, the finding that SNAI2 directly represses BIM, a potent inducer of mitochondrial apoptosis, supports the existence of an exploitable SNAI2/BIM-signaling axis in rhabdomyosarcoma or potentially other tumors with high SNAI2 expression, which could ultimately improve the efficacy of IR therapy in the clinic.

References

- Arndt CA, Crist WM. Common musculoskeletal tumors of childhood and adolescence. *N Engl J Med* 1999;341:342–52.
- Hawkins DS, Gupta AA, Rudzinski ER. What is new in the biology and treatment of pediatric rhabdomyosarcoma? *Curr Opin Pediatr* 2014;26:50–6.
- Hawkins DS, Spunt SL, Skapek SX, Children's Oncology Group Soft Tissue Sarcoma Committee. Children's Oncology Group's 2013 blueprint for research: soft tissue sarcomas. *Pediatr Blood Cancer* 2013;60:1001–8.
- Weigel BJ, Lyden E, Anderson JR, Meyer WH, Parham DM, Rodeberg DA, et al. Intensive multiagent therapy, including dose-compressed cycles of ifosfamide/etoposide and vincristine/doxorubicin/cyclophosphamide, irinotecan, and radiation, in patients with high-risk rhabdomyosarcoma: a report from the Children's Oncology Group. *J Clin Oncol* 2016;34:117–22.
- Borinstein SC, Steppan D, Hayashi M, Loeb DM, Isakoff MS, Binitie O, et al. Consensus and controversies regarding the treatment of rhabdomyosarcoma. *Pediatr Blood Cancer* 2018;65.
- Nieto MA, Huang RY, Jackson RA, Thiery JP. EMT: 2016. *Cell* 2016;166:21–45.
- Shibue T, Weinberg RA. EMT, CSCs, and drug resistance: the mechanistic link and clinical implications. *Nat Rev Clin Oncol* 2017;14:611–29.
- Zhou W, Gross KM, Kuperwasser C. Molecular regulation of Snai2 in development and disease. *J Cell Sci* 2019;132:jcs235127.
- Inoue A, Seidel MG, Wu W, Kamizono S, Ferrando AA, Bronson RT, et al. Slug, a highly conserved zinc finger transcriptional repressor, protects hematopoietic

Authors' Disclosures

N.R. Hensch reports grants from CPRIT and grants from Greehey Family during the conduct of the study. K. Baxi reports grants and other support from NIH T32, NIH TL1, and grants and other support from Greehey Fellowship UTHSCSA during the conduct of the study. M.S. Ignatius reports grants from NCI/NIH, CPRIT, and Voelcker Fund Young Investigator Award. No disclosures were reported by the other authors.

Authors' Contributions

L. Wang: Formal analysis, validation, investigation, visualization, methodology, writing–review and editing. **N.R. Hensch:** Formal analysis, validation, investigation, visualization, methodology, writing–review and editing. **K. Bondra:** Investigation, methodology, writing–review and editing. **P. Sreenivas:** Investigation, visualization, methodology. **X.R. Zhao:** Investigation. **J. Chen:** Investigation, writing–review and editing. **R. Moreno Campos:** Formal analysis, investigation. **K. Baxi:** Investigation, visualization. **A.V. Vaseva:** Resources, validation, writing–review and editing. **B.D. Sunkel:** Formal analysis, validation, writing–review and editing. **B.E. Gryder:** Data curation, software, validation, investigation, visualization, writing–review and editing. **S. Pomella:** Investigation, writing–review and editing. **B.Z. Stanton:** Formal analysis, validation, writing–review and editing. **S. Zheng:** Formal analysis, validation, writing–review and editing. **E.Y. Chen:** Supervision, validation, writing–review and editing. **R. Rota:** Supervision, writing–review and editing. **J. Khan:** Resources, supervision, writing–review and editing. **P.J. Houghton:** Resources, supervision, writing–review and editing. **M.S. Ignatius:** Conceptualization, resources, supervision, funding acquisition, writing–original draft, project administration, writing–review and editing.

Acknowledgments

This project has been funded with federal funds from NIH grants (R00CA175184, NCI P01 CA165995 to M.S. Ignatius and P.J. Houghton) and CPRIT Scholar grant (RR160062 to M.S. Ignatius). M.S. Ignatius is a recipient of the Max and Minnie Tomerlin Voelcker Fund Young Investigator Award. K. Baxi is a T32 and TL1 fellow (T32CA148724, TL1TR002647). N.R. Hensch is a Greehey CCRI Graduate Student Fellow and a CPRIT Predoctoral Fellow (RP 170345).

The costs of publication of this article were defrayed in part by the payment of page charges. This article must therefore be hereby marked *advertisement* in accordance with 18 U.S.C. Section 1734 solely to indicate this fact.

Received December 15, 2020; revised July 13, 2021; accepted August 26, 2021; published first August 30, 2021.

- progenitor cells from radiation-induced apoptosis in vivo. *Cancer Cell* 2002;2:279–88.
- Wu WS, Heinrichs S, Xu D, Garrison SP, Zambetti GP, Adams JM, et al. Slug antagonizes p53-mediated apoptosis of hematopoietic progenitors by repressing puma. *Cell* 2005;123:641–53.
- Erlacher M, Michalak EM, Kelly PN, Labi V, Niederegger H, Coultas L, et al. BH3-only proteins Puma and Bim are rate-limiting for gamma-radiation- and glucocorticoid-induced apoptosis of lymphoid cells in vivo. *Blood* 2005;106:4131–8.
- Gross KM, Zhou W, Breindel JL, Ouyang J, Jin DX, Sokol ES, et al. Loss of slug compromises DNA damage repair and accelerates stem cell aging in mammary epithelium. *Cell Rep* 2019;28:394–407.
- Zhang P, Wei Y, Wang L, Debeb BG, Yuan Y, Zhang J, et al. ATM-mediated stabilization of ZEB1 promotes DNA damage response and radioresistance through CHK1. *Nat Cell Biol* 2014;16:864–75.
- Donehower LA, Soussi T, Korkut A, Liu Y, Schultz A, Cardenas M, et al. Integrated analysis of TP53 gene and pathway alterations in The Cancer Genome Atlas. *Cell Rep* 2019;28:1370–84.
- Olivier M, Hollstein M, Hainaut P. TP53 mutations in human cancers: origins, consequences, and clinical use. *Cold Spring Harb Perspect Biol* 2010;2:a001008.
- Begg AC, Stewart FA, Vens C. Strategies to improve radiotherapy with targeted drugs. *Nat Rev Cancer* 2011;11:239–53.

17. Kirsch DG, Diehn M, Kesarwala AH, Maity A, Morgan MA, Schwarz JK, et al. The future of radiobiology. *J Natl Cancer Inst* 2018;110:329–40.
18. Grobner SN, Worst BC, Weischenfeldt J, Buchhalter I, Kleinheinz K, Rudneva VA, et al. The landscape of genomic alterations across childhood cancers. *Nature* 2018;555:321–7.
19. Chen X, Stewart E, Shelat AA, Qu C, Bahrami A, Hatley M, et al. Targeting oxidative stress in embryonal rhabdomyosarcoma. *Cancer Cell* 2013;24:710–24.
20. Seki M, Nishimura R, Yoshida K, Shimamura T, Shiraishi Y, Sato Y, et al. Integrated genetic and epigenetic analysis defines novel molecular subgroups in rhabdomyosarcoma. *Nat Commun* 2015;6:7557.
21. Shern JF, Chen L, Chmielecki J, Wei JS, Patidar R, Rosenberg M, et al. Comprehensive genomic analysis of rhabdomyosarcoma reveals a landscape of alterations affecting a common genetic axis in fusion-positive and fusion-negative tumors. *Cancer Discov* 2014;4:216–31.
22. Hinson AR, Jones R, Crose LE, Belyea BC, Barr FG, Linardic CM. Human rhabdomyosarcoma cell lines for rhabdomyosarcoma research: utility and pitfalls. *Front Oncol* 2013;3:183.
23. Sokolowski E, Turina CB, Kikuchi K, Langenau DM, Keller C. Proof-of-concept rare cancers in drug development: the case for rhabdomyosarcoma. *Oncogene* 2014;33:1877–89.
24. Houghton PJ, Morton CL, Tucker C, Payne D, Favours E, Cole C, et al. The pediatric preclinical testing program: description of models and early testing results. *Pediatr Blood Cancer* 2007;49:928–40.
25. Gupta PB, Kupervasser C, Brunet JP, Ramaswamy S, Kuo WL, Gray JW, et al. The melanocyte differentiation program predisposes to metastasis after neoplastic transformation. *Nat Genet* 2005;37:1047–54.
26. Schmelzle T, Mailloux AA, Overholtzer M, Carroll JS, Solimini NL, Lightcap ES, et al. Functional role and oncogene-regulated expression of the BH3-only factor Bmf in mammary epithelial anoikis and morphogenesis. *Proc Natl Acad Sci U S A* 2007;104:3787–92.
27. Ignatius MS, Hayes MN, Lobbari R, Chen EY, McCarthy KM, Sreenivas P, et al. The NOTCH1/SNAI1/MEF2C pathway regulates growth and self-renewal in embryonal rhabdomyosarcoma. *Cell Rep* 2017;19:2304–18.
28. Pomella S, Sreenivas P, Gryder BE, Wang L, Milewski D, Cassandri M, et al. Interaction between SNAI2 and MYOD enhances oncogenesis and suppresses differentiation in Fusion Negative Rhabdomyosarcoma. *Nat Commun* 2021;12:192.
29. Woods GM, Bondra K, Chronowski C, Leasure J, Singh M, Hensley L, et al. Radiation therapy may increase metastatic potential in alveolar rhabdomyosarcoma. *Pediatr Blood Cancer* 2015;62:1550–4.
30. Shao L, Sun Y, Zhang Z, Feng W, Gao Y, Cai Z, et al. Deletion of proapoptotic Puma selectively protects hematopoietic stem and progenitor cells against high-dose radiation. *Blood* 2010;115:4707–14.
31. MacQuarrie KL, Yao Z, Fong AP, Diede SJ, Rudzinski ER, Hawkins DS, et al. Comparison of genome-wide binding of MyoD in normal human myogenic cells and rhabdomyosarcomas identifies regional and local suppression of promyogenic transcription factors. *Mol Cell Biol* 2013;33:773–84.
32. Otten AD, Firpo EJ, Gerber AN, Brody LL, Roberts JM, Tapscott SJ. Inactivation of MyoD-mediated expression of p21 in tumor cell lines. *Cell Growth Differ* 1997;8:1151–60.
33. Sharma A, Singh K, Almasan A. Histone H2AX phosphorylation: a marker for DNA damage. *Methods Mol Biol* 2012;920:613–26.
34. Keller C, Arenkiel BR, Coffin CM, El-Bardeesy N, DePinho RA, Capecchi MR. Alveolar rhabdomyosarcomas in conditional Pax3:Fkhr mice: cooperativity of Ink4a/ARF and Trp53 loss of function. *Genes Dev* 2004;18:2614–26.
35. Felix CA, Kappel CC, Mitsudomi T, Nau MM, Tsokos M, Crouch GD, et al. Frequency and diversity of p53 mutations in childhood rhabdomyosarcoma. *Cancer Res* 1992;52:2243.
36. Erlacher M, Labi V, Manzl C, Bock G, Tzankov A, Hacker G, et al. Puma cooperates with Bim, the rate-limiting BH3-only protein in cell death during lymphocyte development, in apoptosis induction. *J Exp Med* 2006;203:2939–51.
37. Kelly PN, White MJ, Goschnick MW, Fairfax KA, Tarlinton DM, Kinkel SA, et al. Individual and overlapping roles of BH3-only proteins Bim and Bad in apoptosis of lymphocytes and platelets and in suppression of thymic lymphoma development. *Cell Death Differ* 2010;17:1655–64.
38. Labi V, Bertele D, Woess C, Tischner D, Bock FJ, Schwemmers S, et al. Haematopoietic stem cell survival and transplantation efficacy is limited by the BH3-only proteins Bim and Bmf. *EMBO Mol Med* 2013;5:122–36.
39. Guo Y, Schoell MC, Freeman RS. The von Hippel-Lindau protein sensitizes renal carcinoma cells to apoptotic stimuli through stabilization of BIM(EL). *Oncogene* 2009;28:1864–74.
40. Wang M, Han J, Marcar L, Black J, Liu Q, Li X, et al. Radiation resistance in KRAS-mutated lung cancer is enabled by stem-like properties mediated by an osteopontin-EGFR pathway. *Cancer Res* 2017;77:2018–28.
41. Khan J, Bittner ML, Saal LH, Teichmann U, Azorsa DO, Gooden GC, et al. cDNA microarrays detect activation of a myogenic transcription program by the PAX3-FKHR fusion oncogene. *Proc Natl Acad Sci U S A* 1999;96:13264–9.
42. Gryder BE, Yohe ME, Chou HC, Zhang X, Marques J, Wachtel M, et al. PAX3-FOXO1 establishes myogenic super enhancers and confers BET bromodomain vulnerability. *Cancer Discov* 2017;7:884–99.
43. Chen EL, Yoo CH, Gutkin PM, Merriott DJ, Avedian RS, Steffner RJ, et al. Outcomes for pediatric patients with osteosarcoma treated with palliative radiotherapy. *Pediatr Blood Cancer* 2020;67:e27967.
44. Zuch D, Giang AH, Shapovalov Y, Schwarz E, Rosier R, O'Keefe R, et al. Targeting radioresistant osteosarcoma cells with parthenolide. *J Cell Biochem* 2012;113:1282–91.
45. Brown LC, Lester RA, Grams MP, Haddock MG, Olivier KR, Arndt CA, et al. Stereotactic body radiotherapy for metastatic and recurrent ewing sarcoma and osteosarcoma. *Sarcoma* 2014;2014:418270.
46. DeLaney TF, Park L, Goldberg SI, Hug EB, Liebsch NJ, Munzenrider JE, et al. Radiotherapy for local control of osteosarcoma. *Int J Radiat Oncol Biol Phys* 2005;61:492–8.
47. Matsunobu A, Imai R, Kamada T, Imaizumi T, Tsuji H, Tsujii H, et al. Impact of carbon ion radiotherapy for unresectable osteosarcoma of the trunk. *Cancer* 2012;118:4555–63.
48. Nieto MA, Sargent MG, Wilkinson DG, Cooke J. Control of cell behavior during vertebrate development by Slug, a zinc finger gene. *Science* 1994;264:835–9.
49. Ros MA, Sefton M, Nieto MA. Slug, a zinc finger gene previously implicated in the early patterning of the mesoderm and the neural crest, is also involved in chick limb development. *Development* 1997;124:1821–9.